

### Simultaneous Noncontact Topography and Electrochemical Imaging by SECM/SICM Featuring Ion Current Feedback Regulation

Yasufumi Takahashi,<sup>†</sup> Andrew I. Shevchuk,<sup>‡</sup> Pavel Novak,<sup>‡</sup> Yumi Murakami,<sup>†</sup>  
Hitoshi Shiku,<sup>†</sup> Yuri E. Korchev,<sup>\*,‡</sup> and Tomokazu Matsue<sup>\*,†</sup>

Graduate School of Environmental Studies, Tohoku University, Aramaki Aoba 6-6-11-605,  
Sendai 980-8579, Japan, and Division of Medicine, Imperial College London, Hammersmith  
Hospital Campus, London W12 0NN, United Kingdom

Received April 9, 2010; E-mail: matsue@bioinfo.che.tohoku.ac.jp

**Abstract:** We described a hybrid system of scanning electrochemical microscopy (SECM) and scanning ion conductance microscopy (SICM) with ion current feedback nanopositioning control for simultaneous imaging of noncontact topography and spatial distribution of electrochemical species. A nanopipette/nanoring electrode probe provided submicrometer resolution of the electrochemical measurement on surfaces with complex topology. The SECM/SICM probe had an aperture radius of 220 nm. The inner and outer radii of the SECM Au nanoring electrode were 330 and 550 nm, respectively. Characterization of the probe was performed with scanning electron microscopy (SEM), cyclic voltammetry (CV), and approach curve measurements. SECM/SICM was applied to simultaneous imaging of topography and electrochemical responses of enzymes (horse radish peroxidase (HRP) and glucose oxidase (GOD)) and single live cells (A6 cells, superior cervical ganglion (SCG) cells, and cardiac myocytes). The measurements revealed the distribution of activity of the enzyme spots on uneven surfaces with submicrometer resolution. SECM/SICM acquired high resolution topographic images of cells together with the map of electrochemical signals. This combined technique was also applied to the evaluation of the permeation property of electroactive species through cellular membranes.

#### Introduction

A high temporal and spatial resolution analytical tool working in physiological conditions is needed to evaluate the relationship of the localized topography and function of biomolecules. Scanning electrochemical microscopy (SECM) uses a micro- or nanoelectrode as a scanning probe and provides sample surface electrochemical property under physiological conditions without physical contact. SECM has been applied for evaluating the enzyme<sup>1–6</sup> and cellular activity,<sup>7,8</sup> estimating cell membrane permeability,<sup>9–18</sup> and detecting electroactive metabolic chemi-

cals with short life spans, such as neurotransmitters<sup>19,20</sup> and nitric oxide (NO)<sup>21</sup> in the vicinity of living cellular surfaces. Membrane protein has also been detected with SECM.<sup>22</sup> Miniaturization of the probe electrode is important for improving the temporal and spatial resolution. In addition, a fine distance regulation system is required to approach the probe electrode against live cell surfaces.

<sup>†</sup> Tohoku University.

<sup>‡</sup> Imperial College London.

- (1) Wittstock, G. *Fresenius J. Anal. Chem.* **2001**, 370, 303–315.
- (2) Luo, H. Q.; Shiku, H.; Kumagai, A.; Takahashi, Y.; Yasukawa, T.; Matsue, T. *Electrochem. Commun.* **2007**, 9, 2703–2708.
- (3) Lei, R.; Stratmann, L.; Schafer, D.; Erichsen, T.; Neugebauer, S.; Li, N.; Schuhmann, W. *Anal. Chem.* **2009**, 81, 5070–5074.
- (4) Schafer, D.; Maciejewska, M.; Schuhmann, W. *Biosens. Bioelectron.* **2007**, 22, 1887–1895.
- (5) Maciejewska, M.; Schafer, D.; Schuhmann, W. *Electroanalysis* **2006**, 18, 1916–1928.
- (6) Hussien, E. M.; Erichsen, T.; Schuhmann, W.; Maciejewska, M. *Anal. Bioanal. Chem.* **2008**, 391, 1773–1782.
- (7) Li, X.; Bard, A. J. *J. Electroanal. Chem.* **2009**, 628, 35–42.
- (8) Takahashi, Y.; Hirano, Y.; Yasukawa, T.; Shiku, H.; Yamada, H.; Matsue, T. *Langmuir* **2006**, 22, 10299–10306.
- (9) Yasukawa, T.; Uchida, I.; Matsue, T. *Biochim. Biophys. Acta Biomembr.* **1998**, 1369, 152–158.
- (10) Barker, A. L.; Macpherson, J. V.; Slevin, C. J.; Unwin, P. R. *J. Phys. Chem. B* **1998**, 102, 1586–1598.

- (11) Gonsalves, M.; Barker, A. L.; Macpherson, J. V.; Unwin, P. R.; O'Hare, D.; Winlove, C. P. *Biophys. J.* **2000**, 78, 1578–1588.
- (12) Cannan, S.; Zhang, J.; Grunfeld, F.; Unwin, P. R. *Langmuir* **2004**, 20, 701–707.
- (13) Liu, B.; Rotenberg, S. A.; Mirkin, M. V. *Proc. Natl. Acad. Sci. U.S.A.* **2000**, 97, 9855–9860.
- (14) Liu, B.; Cheng, W.; Rotenberg, S. A.; Mirkin, M. V. *J. Electroanal. Chem.* **2001**, 500, 590–597.
- (15) Cai, C.; Liu, B.; Mirkin, M. V.; Frank, H. A.; Rusling, J. F. *Anal. Chem.* **2002**, 74, 114–119.
- (16) Liu, B.; Rotenberg, S. A.; Mirkin, M. V. *Anal. Chem.* **2002**, 74, 6340–6348.
- (17) Feng, W.; Rotenberg, S. A.; Mirkin, M. V. *Anal. Chem.* **2003**, 75, 4148–4154.
- (18) Sun, P.; Laforge, F. O.; Abeyweera, T. P.; Rotenberg, S. A.; Carpino, J.; Mirkin, M. V. *Proc. Natl. Acad. Sci. U.S.A.* **2008**, 105, 443–448.
- (19) Hengstenberg, A.; Blochl, A.; Dietzel, I. D.; Schuhmann, W. *Angew. Chem., Int. Ed.* **2001**, 40, 905–908.
- (20) Kurulugama, R. T.; Wipf, D. O.; Takacs, S. A.; Pongmayteegul, S.; Garriss, P. A.; Baur, J. E. *Anal. Chem.* **2005**, 77, 1111–1117.
- (21) Isik, S.; Schuhmann, W. *Angew. Chem., Int. Ed.* **2006**, 45, 7451–7454.
- (22) Takahashi, Y.; Miyamoto, T.; Shiku, H.; Asano, R.; Yasukawa, T.; Kumagai, I.; Matsue, T. *Anal. Chem.* **2009**, 81, 2785–2790.

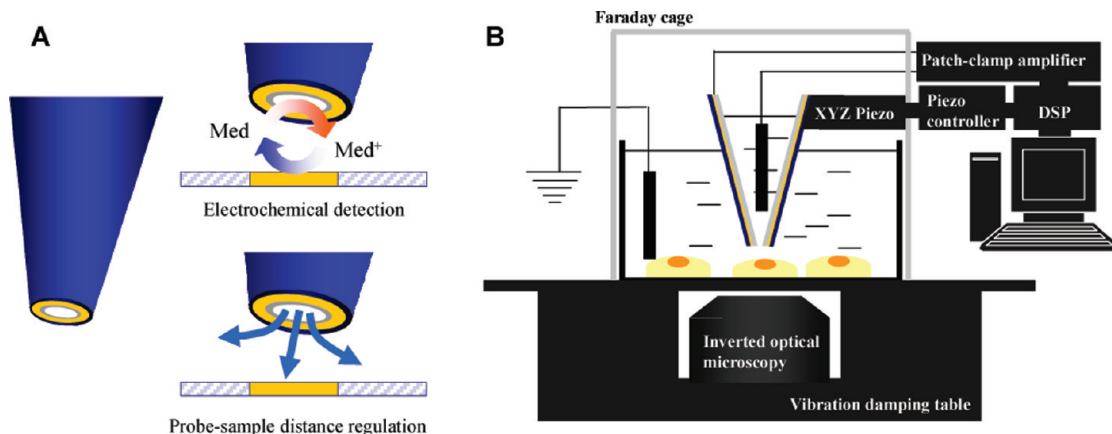


**Figure 1.** (A) Schematic illustration of the SECM/SICM system probe and (B) the SECM/SICM setup.

Significant efforts have been made to bring the electrode proximate with the sample surface using AFM,<sup>23–26</sup> shear force,<sup>8,19,27</sup> and impedance.<sup>20</sup> An electrode-patterned cantilever for the AFM/SECM system was fabricated and applied to simultaneous measurements. Carbon nanotube,<sup>24</sup> high resistive polymer,<sup>25</sup> and nanofabrication technique<sup>26</sup> have been adapted for making high aspect ratio shape probes. Nevertheless, it was difficult to apply the system to the measurement of soft samples because the force interaction was usually very unstable to serve as a feedback signal. The degradation of the electrochemical sensitivity caused by undesired electrochemical reactions at the side surfaces of the cantilever is also a problem. Shear force feedback regulation has also been used for control of the probe electrode sample distance. Previously, we reported the simultaneous imaging of the topography and electrochemical signals of single living cells using shear force distance regulation of a ring-type nanoelectrode probe.<sup>27</sup> However, preventing probe–cell contact was still difficult because the solution viscosity interfered with the shear force detection. Impedance-based probe–sample distance regulation has been used as a feedback mechanism for noncontact living cell imaging; however, it is difficult to improve the resolution of topography imaging because miniaturization of the electrode degrades the resistance signals for regulating the probe–sample distance.

Scanning ion conductance microscopy (SICM) uses a nanopipette as a scanning probe and provides living cell surface topography images under physiological conditions without physical contact.<sup>28</sup> Recent advances in SICM resulted in the development of a novel hopping probe ion conductance microscopy (HPICM) that allows topographical imaging of most convoluted surfaces.<sup>29</sup> SICM is based on the phenomenon that the ion flow through a sharp fluid-filled nanopipette is partially occluded when the nanopipette approaches the surface of a sample. Living cell surface topography and dynamic measurements have been performed. Topographical information of the live cell surface can be used to improve the resolution of other analytical tools; SICM nanopositioning system was combined with near field scanning optical microscopy,<sup>30</sup> confocal microscopy,<sup>31</sup> and patch clamps.<sup>32,33</sup> The nanopipette not only can detect localized ions but can also provide specific ion and biomolecules in a localized place.<sup>34</sup>

Hersam and co-workers reported combining SECM and SICM and demonstrated simultaneous submicrometer resolution topography and electrochemical imaging of gold film electrodes.<sup>35</sup> They used atomic layer deposition (ALD) of aluminum oxide to

conformally insulate a gold-coated nanopipette and focused ion beam (FIB) milling to precisely expose the electrode surface. Bard et al. reported a similar probe design to dispense small amounts of a solution while monitoring the electrochemical response.<sup>36</sup>

In this work, we demonstrate a hybrid system of SECM and HPICM for simultaneous imaging of topography and electrochemical signal. This system is particularly suitable for detailed characterization of soft biomaterials with complex 3D structures, such as live cells. Figure 1 shows the structure of a nanopipette/nanoring electrode probe and a schematic diagram of the SECM/SICM measurement setup. Ion current flowing between Ag/AgCl electrodes located inside the nanopipette and the outside solution was used as the feedback signal for distance control. The electrochemical signal was acquired with the nanoring electrode. The present study demonstrates that the SECM/SICM system can generate submicrometer resolution images based on topography and electrochemical signals of enzymes on solid surfaces and convoluted living cells. The system was also found to be applicable

- (23) Macpherson, J. V.; Unwin, P. R.; Hillier, A. C.; Bard, A. J. *J. Am. Chem. Soc.* **1996**, *118*, 6445–6452.
- (24) Burt, D. P.; Wilson, N. R.; Weaver, J. M. R.; Dobson, P. S.; Macpherson, J. V. *Nano Lett.* **2005**, *5*, 639–643.
- (25) Patil, A.; Sippel, J.; Martin, G. W.; Rinzler, A. G. *Nano Lett.* **2004**, *4*, 303–308.
- (26) Shin, H.; Hesketh, P. J.; Mizaikoff, B.; Kranz, C. *Anal. Chem.* **2007**, *79*, 4769–4777.
- (27) Takahashi, Y.; Shiku, H.; Murata, T.; Yasukawa, T.; Matsue, T. *Anal. Chem.* **2009**, *81*, 9674–9681.
- (28) Korchev, Y. E.; Bashford, C. L.; Milovanovic, M.; Vodyanoy, I.; Lab, M. J. *Biophys. J.* **1997**, *73*, 653–658.
- (29) Novak, P.; Li, C.; Shevchuk, A. I.; Stepanyan, R.; Caldwell, M.; Hughes, S.; Smart, T. G.; Gorelik, J.; Ostanin, V. P.; Lab, M. J.; Moss, G. W.; Frolenkov, G. I.; Klenerman, D.; Korchev, Y. E. *Nat. Methods* **2009**, *6*, 279–281.
- (30) Korchev, Y. E.; Raval, M.; Lab, M. J.; Gorelik, J.; Edwards, C. R. W.; Rayment, T.; Klenerman, D. *Biophys. J.* **2000**, *78*, 2675–2679.
- (31) Gorelik, J.; Shevchuk, A.; Ramalho, M.; Elliott, M.; Lei, C.; Higgins, C. F.; Lab, M. J.; Klenerman, D.; Krauszewicz, N.; Korchev, Y. *Proc. Natl. Acad. Sci. U.S.A.* **2002**, *99*, 16018–16023.
- (32) Korchev, Y. E.; Negulyaev, Y. A.; Edwards, C. R. W.; Vodyanoy, I.; Lab, M. J. *Nat. Cell Biol.* **2000**, *2*, 616–619.
- (33) Gorelik, J.; Gu, Y. C.; Spohr, H. A.; Shevchuk, A. I.; Lab, M. J.; Harding, S. E.; Edwards, C. R. W.; Whitaker, M.; Moss, G. W. J.; Benton, D. C. H.; Sanchez, D.; Darszon, A.; Vodyanoy, I.; Klenerman, D.; Korchev, Y. E. *Biophys. J.* **2002**, *83*, 3296–3303.
- (34) Piper, J. D.; Li, C.; Lo, C. J.; Berry, R.; Korchev, Y.; Ying, L. M.; Klenerman, D. *J. Am. Chem. Soc.* **2008**, *130*, 10386–10393.
- (35) Comstock, D. J.; Elam, J. W.; Pellin, M. J.; Hersam, M. C. *Anal. Chem.* **2010**, *82*, 1270–1276.
- (36) Walsh, D. A.; Fernandez, J. L.; Mauzeroll, J.; Bard, A. J. *Anal. Chem.* **2005**, *77*, 5182–5188.

for evaluating the permeation property of electroactive species through cellular membranes. To our knowledge, this is the first report of high-resolution imaging of biomaterials with SECM/SICM.

## Material and Methods

**Reagents.** Glucose oxidase (GOD; Biozyme Laboratories), horse radish peroxidase (HRP; Wako), L-15 medium (Gibco, Parsippany, NJ), ferrocenylmethanol ( $\text{FcCH}_2\text{OH}$ ; Aldrich), potassium hexacyanoferrate (II) trihydrate ( $\text{K}_4\text{Fe}(\text{CN})_6 \cdot 3\text{H}_2\text{O}$ ; Kanto Chemical Co., Inc.), glutaraldehyde (GA; Wako), and bovine serum albumin (BSA; Wako) were purchased and used as received. PBS was prepared from 7.2 mM  $\text{Na}_2\text{HPO}_4 \cdot 12\text{H}_2\text{O}$ , 2.8 mM  $\text{KH}_2\text{PO}_4$ , and 150 mM NaCl (pH 7.0).

**Fabrication of the SECM/SICM Electrode.** A glass capillary (World Precision Instruments, Inc., PG10165-4) was pulled using a capillary puller (Narishige PE-21). This capillary was then coated by Ti/Pt or Ti/Au sputtering (Anelva, L-332S-FH, RF200), followed by insulation with an anodic electrophoretic paint (Elecoat AE-X, Shimizu Co., Ltd.) by immersing the top of the metal-coated capillary and applying a DC potential of +2.0 V for 2 min between the capillary and counter electrode. After electrophoretic deposition, the electrode was removed from the solution, washed for 10 s to remove excess paint solution, and cured in an oven for 45 min at 150 °C to harden the insulation layer. To expose an electroactive area and form an ion transport aperture, the probe apex was milled by a focused ion beam (FIB, Seiko Instruments, SMI 2050).

**Preparation of the Enzyme Spot.** A PBS solution containing 1 mg/mL enzyme, 5 mg/mL BSA, and 1% GA was spotted on an APS-coated glass slide (Matsunami Glass Ind., Ltd.) and dried in air for 30 min.

**Cell Culture and Isolation.** A single A6 cell line was kindly provided by Dr. P. DeSmet (Karnolieke Universiteit, Belgium). All experiments were performed between 127 and 134 passages. Cells were cultured, as described previously.<sup>37</sup>

Superior cervical ganglion (SCG) cells were kindly provided by Dr. Guy Moss. Cells were cultured at a high density ( $9 \times 10^5$  cells/mL) on poly-L-lysine-coated coverslips. Cells were kept in a growth medium consisting of a DMEM (Gibco) supplemented with 10% fetal bovine serum (Gibco), 100  $\mu\text{g}/\text{mL}$  streptomycin and 100 U/mL penicillin (Gibco), nerve growth factor (67 ng/mL, 2.5 S; Gibco). Cells were maintained at 37 °C in an atmosphere of humidified air with 95%  $\text{O}_2$ /5%  $\text{CO}_2$ . Cells were used for SECM/SICM measurements after 2–5 days when they had migrated to form cell clusters connected by axon bundles.

Cardiac myocytes from adult rats were isolated by digestion of intact perfused ventricle, according to the method previously described.<sup>38</sup>

**Instrumentation.** Figure 1B shows a schematic diagram of the SECM/SICM instrument, which has been previously described.<sup>32</sup> The currents were measured with a dual channel MultiClamp700B patch-clamp amplifier (Axon Instruments). The electrochemical and ion current signals were low-pass filtered at 40 Hz and 1 kHz, respectively. The data was digitized and analyzed with continuous data acquisition hardware and software (Axon Digidata 1322A, Axon Instruments). The probe position was controlled by a XY and Z piezoelectric scanner (Physik Instrumente, 621.2CL and 621.ZCL), which was controlled with an amplifier module (Physik Instrumente, E-503.00) and servo control module (Physik Instrumente, E-509.C3). The system was controlled by a program written with Delphi (Borland) and Code Composer Studio (Texas Instruments, U.S.A.) for ScanIC controller (Ionscope, UK).

**SECM/SICM Measurements.** The nanopipette electrode brought near the sample surface used ion current as the feedback signal and acquired height information. The electrochemical measurement was performed by the nanoring electrode. A hopping mode<sup>29</sup> was adopted as the scanning method. Briefly, the vertical Z positioning of the hopping probe and the movement of the sample in the XY plane were controlled at a sampling frequency of 20 kHz. A five-step procedure was used to determine the height and detect electrochemical species of the specimen at each imaging point. First, the probe was withdrawn a specified distance from its existing position. Second, the vertical position of the probe was maintained for 10 ms, while the nanopositioning stage moved to a new imaging point in the XY plane. During this time a reference current,  $I_{\text{REF}}$ , was measured as an average of the DC current through the probe. Third, the probe was lowered at constant fall rate of 15 nm/ms while monitoring the difference in the current,  $I$ , between  $I_{\text{REF}}$  and the instantaneous current through the probe  $I_{\text{MV}}$ . As soon as  $I$  drop exceeded the specified value of the set point,  $I_s$ , which was approximately 1.0–1.5% of  $I_{\text{REF}}$ , the vertical position of the probe was saved into the corresponding image pixel. Fourth, electrochemical measurement was performed for 200  $\mu\text{s}$  using the nanoring electrode. Finally, the probe was quickly withdrawn by a specified hop amplitude to start a new measurement cycle.

## Results and Discussion

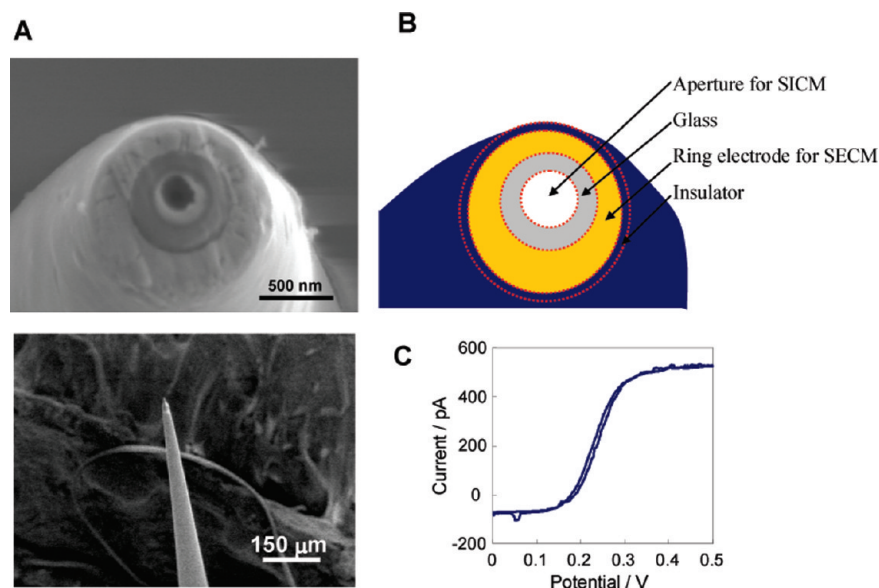
**Characterization of the SECM/SICM Probe.** Panels A and B of Figure 2 show the SEM images and the structure of the SECM/SICM probe apex, respectively. The nanopipette aperture radius was found to be 220 nm. The Au nanoring electrode for SECM measurements was fabricated outside of the glass sheath, and the inner and outer radii of the nanoring electrode were found to be 330 and 550 nm, respectively. The SECM nanoring electrode was coated with a 70 nm thick insulator film. The probe angle was less than 10°, which allowed the probe to access a relatively high aspect sample. Figure 2C shows a cyclic voltammogram (CV) of 0.50 mM ferrocenylmethanol ( $\text{FcCH}_2\text{OH}$ ), observed on the SECM nanoring electrode in 0.1 M KCl at a scanning rate of 100 mV/s. The voltammogram shows a sigmoidal shape with the steady-state current of 500 pA, which is approximately 6 times larger than that expected for a microdisk electrode with the same electrode size. The larger current is probably due to defects in the insulating layer. The defects did not cause a serious problem in SECM imaging based on generation collection (GC) and feedback (FB) measurements, as shown later. The SECM/SICM probe with a SECM Pt nanoring electrode also showed similar electrochemical behavior. Since the Pt nanoring electrode showed undesirable electrochemical responses in  $\text{H}_2\text{O}_2$  solution, the probe with an Au nanoring electrode was used for imaging in  $\text{H}_2\text{O}_2$  solutions, as described later.

Figure 3 shows approach curves to conductive and insulating substrates. The potentials of the SECM Pt and SICM Ag/AgCl electrodes were set at 500 and 200 mV, respectively. In either case, the ion current signal decreased as the tip approached the sample surface ( $z \rightarrow 0$ ), which illustrates the fundamental nature of the ion current, blocked by either electron-insulating or electron-conducting surfaces. The distance for a 1% change of the SICM response (ion current) was almost the same as the nanopipette inner radius, in this case 220 nm. The experimental results were in good agreement with theory classified in reference 28. On the other hand, the approach curves of the electrochemical current signal for the insulating and conducting substrates showed negative and positive feedback features, respectively. The change in the electrochemical current was small probably due to the electrochemical reaction through the defects of the probe insulating wall. Importantly, no interference

(37) Gorelik, J.; Shevchuk, A. I.; Frolenkov, G. I.; Diakonov, I. A.; Lab, M. J.; Kros, C. J.; Richardson, G. P.; Vodyanov, I.; Edwards, C. R. W.; Klenerman, D.; Korchev, Y. E. *Proc. Natl. Acad. Sci. U.S.A.* **2003**, *100*, 5819–5822.

(38) Lyon, A. R.; MacLeod, K. T.; Zhang, Y.; Garcia, E.; Kanda, G. K.; Lab, M. J.; Korchev, Y. E.; Harding, S. E.; Gorelik, J. *Proc. Natl. Acad. Sci. U.S.A.* **2009**, *106*, 6854–6859.





**Figure 2.** (A) SEM micrographs of the SECM/SICM probe. (B) Schematic illustration of probe structure. (C) Cyclic voltammogram of 0.50 mM  $\text{FcCH}_2\text{OH}$  on a SECM nanoring electrode in a 0.1 M KCl solution at a scanning rate of 100 mV/s. The nanopipette aperture radius was 220 nm. Inner and outer radii of the SECM Au nanoring electrode were 330 and 550 nm, respectively. The insulator was 70 nm thick.

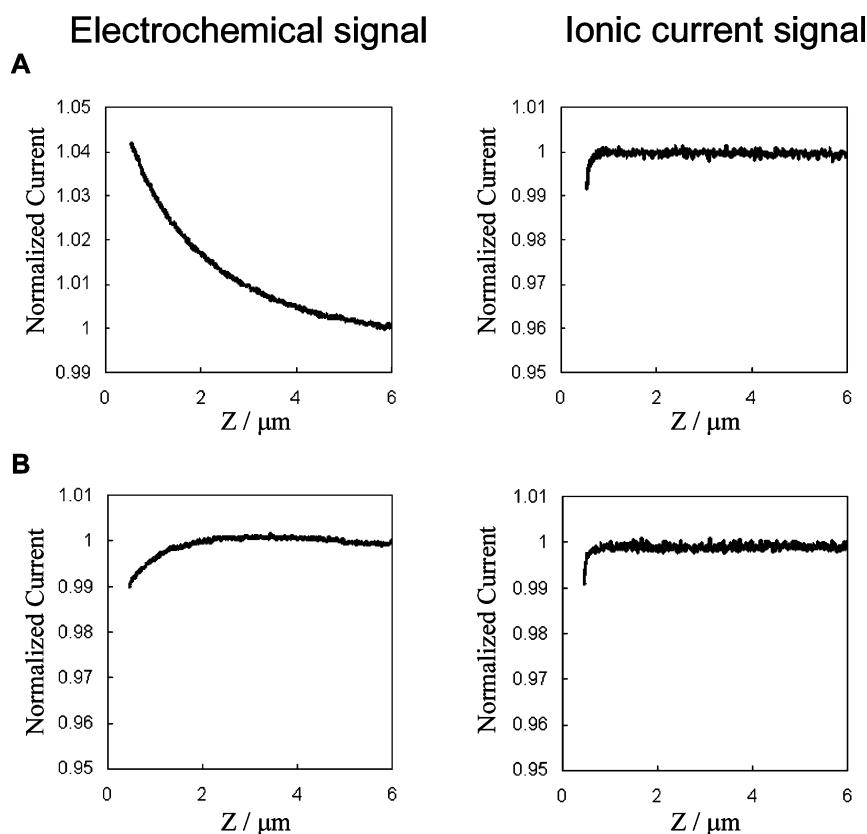


**Figure 3.** Approach curves of a SECM/SICM electrode to a (A) conductive Pt and (B) insulated glass surface in a 0.50 mM  $\text{FcCH}_2\text{OH}$  + 0.1 M KCl solution for simultaneous electrochemical (left) and ion current (right) measurements. The SECM nanoring and SICM nanopipette electrodes were held at 500 and 300 mV vs Ag/AgCl, respectively.

was observed from CV measurements between the ion and electrochemical currents at the electrodes (Supporting Information, Figure S1). This indicated that interference between the nanoring electrode and Ag/AgCl electrode does not occur in simultaneous topographical and electrochemical imaging.

**Imaging a Pt Interdigitated Array Electrode (IDA).** We measured a Pt interdigitated array electrode (IDA) to show the noncontact distance regulation of SECM/SICM. If the probe collides with the IDA during scanning, it may break, resulting in an abrupt ion current increase, making it impossible to

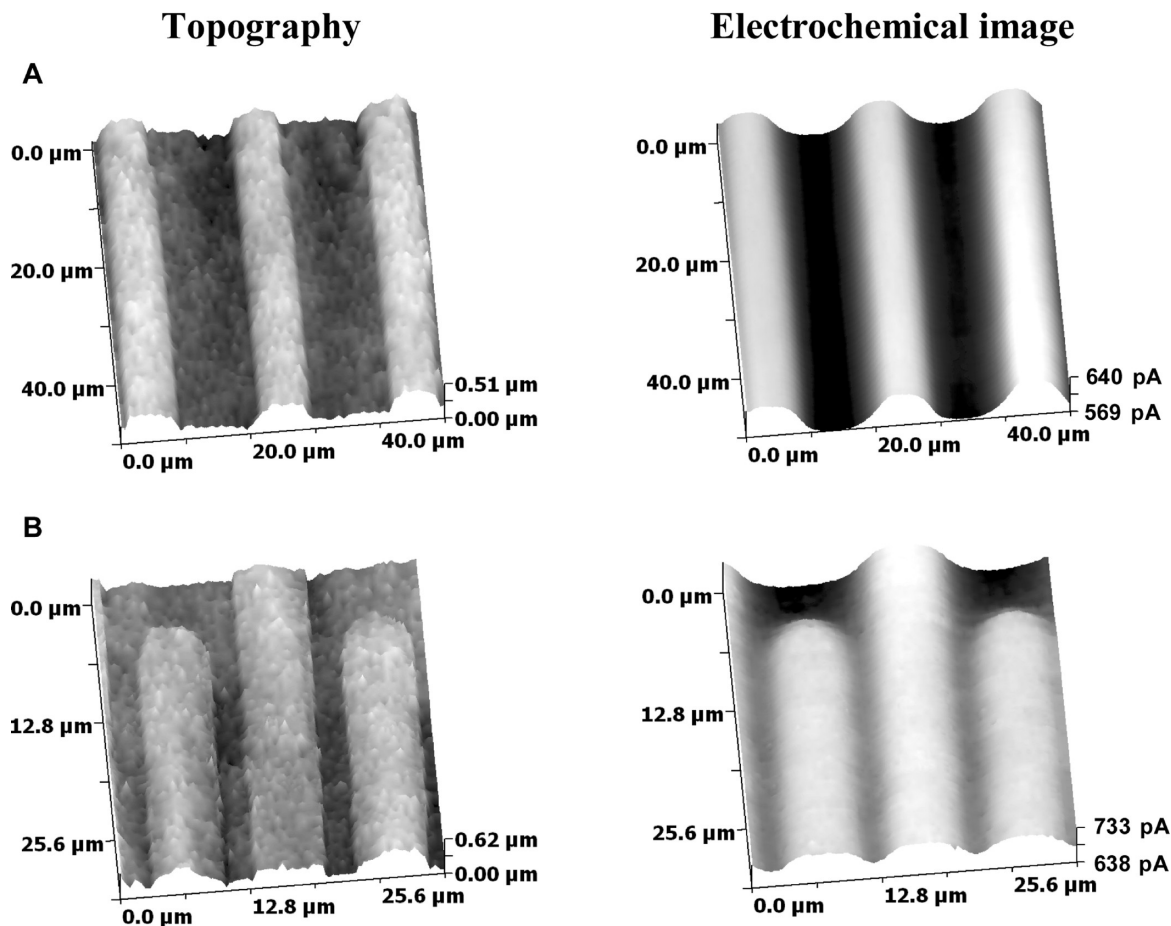


**Figure 4.** Topographic (left) and electrochemical (right) images of a Pt band microarray in 0.50 mM  $\text{FcCH}_2\text{OH}$  + 0.1 M KCl. The SECM nanoring and SICM nanopipette electrodes were held at 500 and 300 mV vs Ag/AgCl, respectively. Scan ranges were (A)  $50\ \mu\text{m} \times 50\ \mu\text{m}$  and (B)  $32\ \mu\text{m} \times 32\ \mu\text{m}$ .

maintain constant distance regulation. Furthermore, the SECM electrochemical current increases if the nanoring electrode contacts and forms a short circuit with the Pt IDA. Figure 4 shows the SECM/SICM images of the Pt IDA in a solution containing 0.50 mM  $\text{FcCH}_2\text{OH}$  and 0.1 M KCl. The potentials of the SECM Pt nanoring and SICM Ag/AgCl electrodes were 500 and 200 mV, respectively. When the probe moved above the Pt IDA, the electrochemical signal increased due to positive feedback resulting from redox cycling; however, an electric short circuit current was not seen. The probe–sample distance was maintained at 300 nm, which was similar to the size of aperture of the probe. From the image, the height of the Pt IDA was found to be 100 nm, which was in good agreement with the size determined by conventional AFM (Supporting Information, Figure S2). These results showed that noncontact simultaneous imaging based on topographic and electrochemical characteristics were possible on a submicrometer scale by using ion current as the feedback signal.

**Enzyme Spot Measurement.** The protein microarray has become a popular tool for high throughput screening of ligand–receptor binding tests. Nanoliter- to subnanoliter-sized droplets of protein solutions are arrayed on a solid surface by a robotic spotter; however, a ringlike structure at the edge of the spot<sup>39</sup> results in heterogeneous distribution of the protein that degrades the sensitivity and reproducibility of the protein

chip. Revealing the localized activity of the enzyme spot would improve the sensitivity and reproducibility of the protein microarray. In the past, patterned monolayer enzyme activity<sup>2</sup> and ringlike structure at the edge of the spot<sup>3</sup> were measured by SECM. Especially, the Schuhmann group reported on enzyme–polymer spots,<sup>4–6</sup> but SECM image resolutions of those reports were not enough to clarify the submicro-scale activity of the localized spotted protein.

We measured a portion of the HRP and GOD spotted pattern using SECM/SICM. HRP and GOD measurements were performed in the substrate generation tip collection (GC) and feedback (FB) modes, respectively. Figure 5 shows the SECM/SICM images of a portion of a HRP spot edge in a PBS solution containing 0.50 mM  $\text{FcCH}_2\text{OH}$ . The potentials of the SECM Au nanoring and SICM Ag/AgCl electrodes were 50 and 200 mV, respectively. The SICM image shows a clear topographic image of the HRP spot with uneven surfaces in the center and a ring-like range at the edge. The height of the edge of HRP spot was found to be approximately 260 nm. The immobilized HRP catalyzes the reduction of  $\text{H}_2\text{O}_2$  by  $\text{FcCH}_2\text{OH}$  to form  $[\text{FcCH}_2\text{OH}]^+$ , which is reduced back to  $\text{FcCH}_2\text{OH}$  at the SECM nanoring electrode. Before adding  $\text{H}_2\text{O}_2$ , the reduction current was not seen at all (Figure 5A right image), while the apparent reduction current of  $[\text{FcCH}_2\text{OH}]^+$  was detected after addition of 0.50 mM  $\text{H}_2\text{O}_2$  (Figure 5B right image). The SECM image shows the increased reduction current, especially at the edge of the HRP spot, which is in good agreement with the topographic image obtained by SICM. The GC mode is known as a sensitive

(39) Deng, Y.; Zhu, X. Y.; Kienlen, T.; Guo, A. *J. Am. Chem. Soc.* **2006**, *128*, 2768–2769.

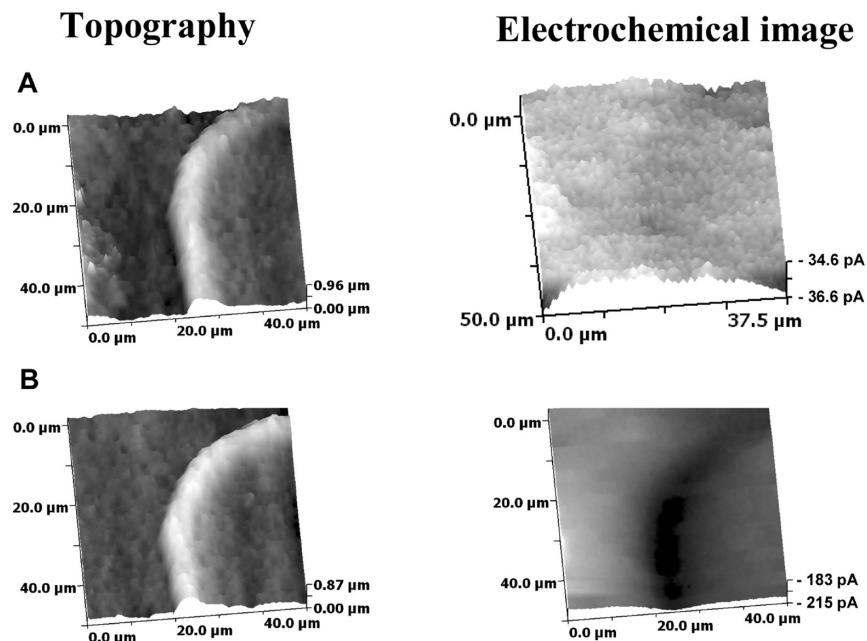


**Figure 5.** Topographic (left) and electrochemical (right) images of a portion of the HRP spot immobilized on a glass substrate (A) before and (B) after adding 0.50 mM  $\text{H}_2\text{O}_2$  in 0.50 mM  $\text{FcCH}_2\text{OH}$  and PBS. The SECM nanoring and SICM nanopipette electrodes were held at 50 and 300 mV vs Ag/AgCl, respectively. Scan ranges were  $50\ \mu\text{m} \times 50\ \mu\text{m}$ .

detection mode because the generation of the redox reaction species is dominated by enzyme activity and the background current is very low. However, it is difficult to improve the spatial resolution using a distance regulation system, even if the microelectrode is positioned near the enzyme, because the steady-state diffusion layer is formed around the enzyme. Therefore, we also performed the FB mode measurement to obtain high-resolution SECM images of enzyme spots. Feature and advantage of enzyme measurement using GC mode and FB mode was reported by Wittstock.<sup>1</sup>

Figure 6 shows the SECM/SICM images of a portion of the GOD spot in a PBS solution containing 0.50 mM  $\text{FcCH}_2\text{OH}$ . The potentials of the SECM Pt nanoring and SICM Ag/AgCl electrodes were 500 and 200 mV, respectively. At the SECM nanoring electrode,  $\text{FcCH}_2\text{OH}$  is oxidized to  $[\text{FcCH}_2\text{OH}]^+$ , which diffuses to the surface of the GOD spot. GOD on the substrate catalyzes the oxidation of glucose and the reduction of  $[\text{FcCH}_2\text{OH}]^+$  to  $\text{FcCH}_2\text{OH}$  diffusing back to the SECM. When the electrode is near the GOD, redox cycling of  $[\text{FcCH}_2\text{OH}]^+/\text{FcCH}_2\text{OH}$  occurred to amplify the electrochemical current. Panels A and B of Figure 6 show the SICM and SECM images before adding glucose. The topographic image from SICM indicates the ringlike structure of the GOD spot with an edge height of approximately 200 nm. The SECM image without glucose showed small differences in the oxidation current along the edge, probably due to negative feedback caused by the edge. Figure 6C shows the SECM images after adding 20 mM glucose. The increase in  $\text{FcCH}_2\text{OH}$  oxidation current associated with GOD-catalyzed reaction was seen, and the electrochemical current profile was in good agreement with the topographic image of the GOD spot.

We also investigated interference between the SECM nanoring and SICM Ag/AgCl electrodes. Figure 6D shows the SECM image when the potential of the Ag/AgCl electrode changed from 200 to  $-200$  mV, while the potential of the SECM nanoring electrode was unchanged at  $+500$  mV. No difference in the SECM image was found before and after changing the potential of the Ag/AgCl electrode (Figures 6C and D). This

indicated that the SECM nanoring and SICM Ag/AgCl electrodes had no interference.

The probe–sample distance was an important parameter for FB mode imaging. Figure 7 shows the SICM topographic and SECM images in which the probe–sample distances were held at 100 and 600 nm. The SICM image showed a highly resolved structure of the GOD spot surface with small caves 320 nm  $\times$  1600 nm in size (Figure 7A). When the distance was set to 100 nm, the SECM image also shows that fine structure with small caves (Figure 7B), but the cave-like structure disappeared in the SECM image at a distance of 600 nm (Figure 7C). These results clearly demonstrate that SICM distance regulation is very effective in improving its resolution in FB imaging. The SECM image with a higher magnification (Figure 7E) clearly shows the single cave with low electrochemical responses. Although the electrode diameter was approximately 700 nm, features as small as 100 nm could be visualized by both SICM topography and SECM images. This is the first time that the enzyme activity has been imaged with nanometer resolution using SECM.

**Topographic Imaging of Live Cells.** The distribution of ion channels and receptors at specific locations on the cell surface plays an important role in signal transduction. Most cell types develop complex structures that form predominant locations for ion channel and receptor clustering. Mapping the distributions of ion channels and receptors on complex surfaces by SECM would not be possible without precise distance control. Therefore, we chose two highly structured cell types, superior cervical ganglion (SCG) cells and A6 cells, to evaluate the topographical resolution of SECM/SICM. Panels A–D of Figure 8 show the optical microscopy image and topographic images of SCG cells. The red square frame of the optical microscopy image shows the scanning area of Figure 8B. By adopting the hopping mode, SECM/SICM could simultaneously image the axon and cell body. Moreover, varicosities, which administrate neuron transduction and axon formation, were seen clearly on the axon (marked by asterisks). D and E of Figure 8 show the topographic images of A6 cells. Ridge-like structures, formed by microvilli, can be seen on the cell surface.

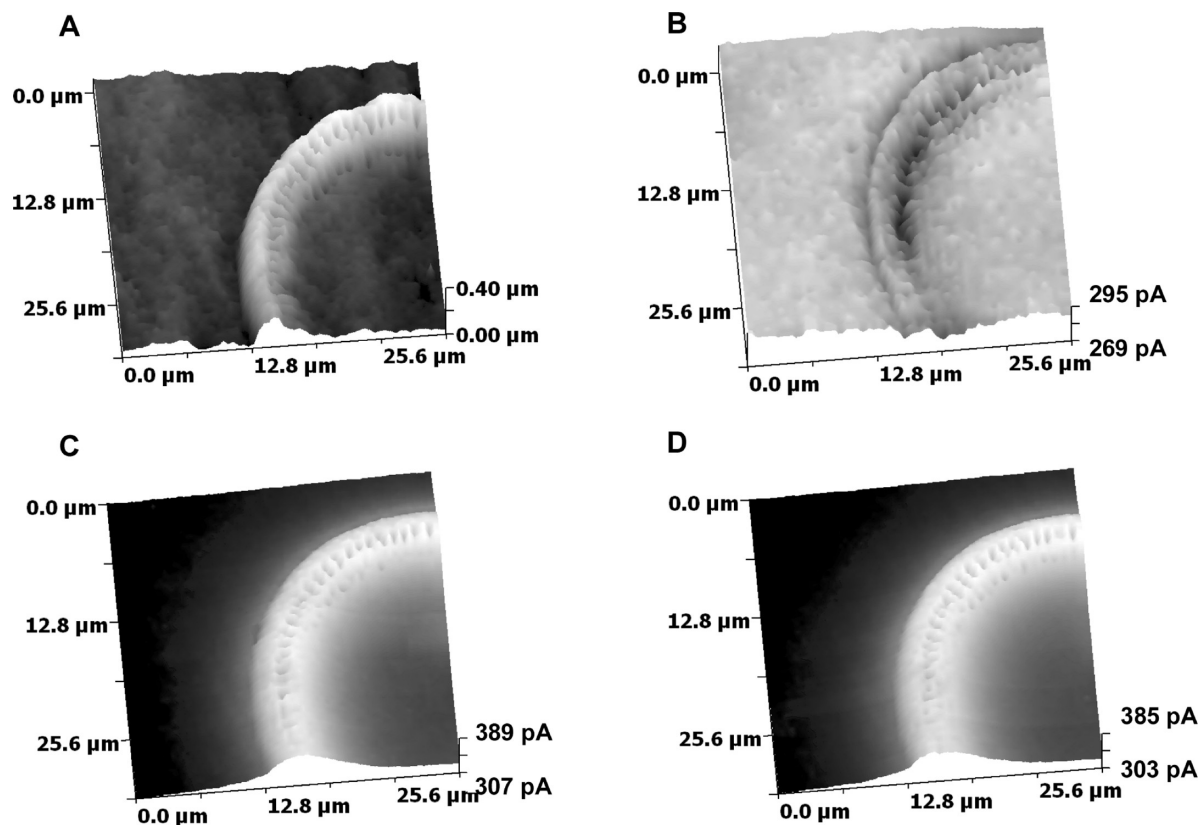


**Figure 6.** (A) Topographic and (B–D) electrochemical images of GOD immobilized substrate (A and B) before and (C and D) after adding 20 mM glucose in 0.50 mM  $\text{FcCH}_2\text{OH}$  + 0.1 M KCl. The SECM nanoring and SICM nanopipette electrodes were held at 500 and 200 mV vs Ag/AgCl, respectively, for (A–C), while the potential of the SICM nanopipette electrode was changed to  $-200$  mV vs Ag/AgCl for (D). Scan ranges were  $32\ \mu\text{m} \times 32\ \mu\text{m}$ .

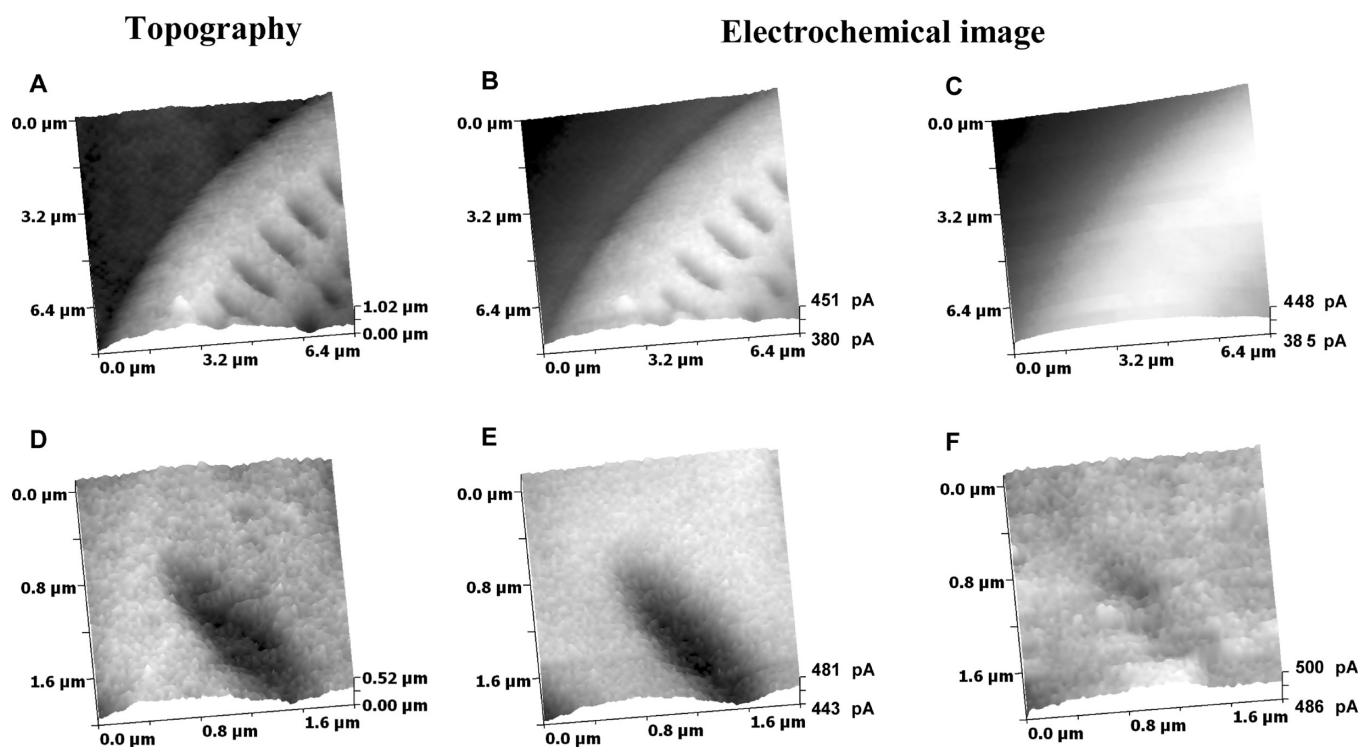


**Figure 7.** (A and D) Topographic and (B, C, E, and F) electrochemical images of a GOD immobilized substrate adding 20 mM glucose in 0.50 mM  $\text{FcCH}_2\text{OH}$  + 0.1 M KCl. The SECM nanoring and SICM nanopipette electrodes were held at 500 and 200 mV vs Ag/AgCl, respectively. Upper and lower images were captured with  $8\ \mu\text{m} \times 8\ \mu\text{m}$  and  $2\ \mu\text{m} \times 2\ \mu\text{m}$ , respectively. The probe–sample distances were held at 100 nm (B and E) and 600 nm (C and F), respectively.



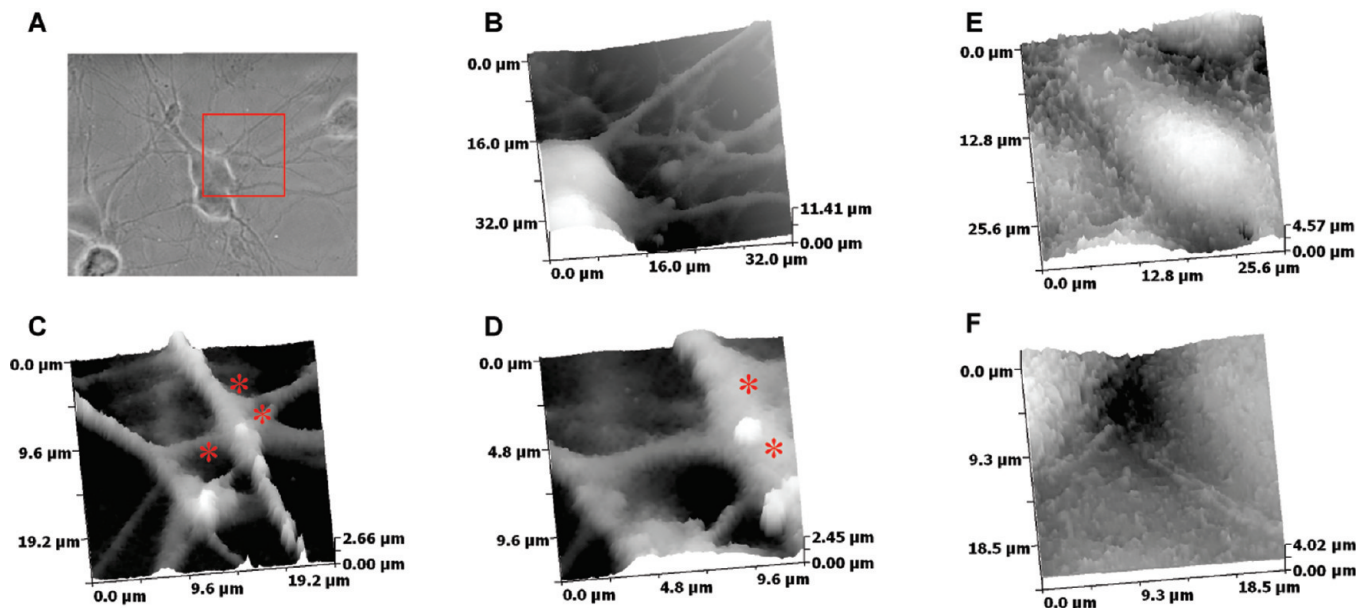


**Figure 8.** (A) Photograph and SICM topographic images of (B–C) SCG cells and (D, E) A6 cells in a culture medium L-15, using a SECM/SICM probe. Scan ranges were (B)  $40\ \mu\text{m} \times 40\ \mu\text{m}$ , (C)  $24\ \mu\text{m} \times 24\ \mu\text{m}$ , (D)  $12\ \mu\text{m} \times 12\ \mu\text{m}$ , (E)  $32\ \mu\text{m} \times 32\ \mu\text{m}$ , and (F)  $23.1\ \mu\text{m} \times 23.1\ \mu\text{m}$ .

At the cell–cell contact region, a tight junction area formed by the double row of microvilli can be seen. This is an important feature for maintaining the function of renal cells. These results indicated that the SECM/SICM probe can resolve the topography of the living cellular surface well beyond submicrometer resolution, and the hopping mode is a suitable SECM distance control for convoluted cell topography imaging.

#### Evaluation of Permeation Property of the Cell Membrane.

The permeation property of the cell membrane plays an important role in intracellular biochemical reactions. SECM is a powerful tool for estimating transport rates of electrochemical species across the liquid/liquid interfaces.<sup>10</sup> Mirkin and other groups reported about electrochemical mediator permeability and electron transfer kinetics of living cells using SECM.<sup>9,11–18</sup> However, several technical challenges still remain unsolved. First, the cell membrane has the possibility of heterogeneous permeability in specific regions; second, biomolecules adsorb to the electrode surface (electrode fouling) and decrease the steady-state current; third, the heterogeneity of the cellular surface affects the approach curve measurement. Most simulations for estimating permeability by fitting experimental data do not consider the surface heterogeneity. It is desirable to acquire an estimation of membrane permeability with the surface topography and continually monitor the approach curves. By adopting the hopping mode, SECM/SICM can acquire the approach curve at each measurement point. Therefore, we evaluated the permeation property on the cell membrane simultaneously with the cell surface topography.

In this experiment, we measured Faradaic current for the oxygen, potassium hexacyanoferrate (II) trihydrate ( $\text{K}_4[\text{Fe}(\text{CN})_6]$ ), and  $\text{FcCH}_2\text{OH}$  on a cardiac myocyte. Figure 9 shows the SICM topographic and SECM images and current profiles at each measurement point on a cardiac myocyte. The arrow shows a direction of the approach, from a start point ( $10\ \mu\text{m}$  above the surface) to the sample surface ( $300\ \text{nm}$  from the surface), which is the end point of the vertical scan. Unfortunately, the topographical resolution of the images was inadequate to visualize the sarcoma structure in detail; however, it was sufficient to visualize the cardiac myocyte shape very clearly.

The cell height was found to exceed  $20\ \mu\text{m}$ . The hopping mode was effective for such high aspect sample topographic measurements. The electrochemical images were shown as a Faradaic current associated with the localized permeation property of a specific chemical. The reduction current of the oxygen (negative value) decreased as the probe approached the sample surface, indicating that the negative feedback effects were seen weakly at the all measuring points. The oxygen reduction current at the cellular membrane surface ( $3.6\ \mu\text{m} < X < 7.0\ \mu\text{m}$ ) was clearly large compared with that at the surface of the culture dish ( $X < 3.6\ \mu\text{m}$ ;  $7.0\ \mu\text{m} < X$ ) (Figure 9A right image). This indicated that the cell membrane has a high permeability for oxygen. It is noteworthy that the current contrast changed, depending on the SECM probe electrode size and the probe scanning rate.<sup>22</sup> Therefore, a very small electrode is preferential to separately characterize the local oxygen concentration and the membrane permeation property.<sup>8</sup>

When monitoring  $[\text{Fe}(\text{CN})_6]^{4-}$  oxidation current (positive value), the oxidation current decreases as the probe repeatedly approaches the sample surface, due to the negative feedback effects.  $[\text{Fe}(\text{CN})_6]^{4-}$  is a hydrophilic mediator and cannot cross the cell membrane. At the end point of the vertical scans, the oxidation currents were seen at the same level for a cellular surface and substrate (Figure 9B right image). This indicates that the diffusion of  $[\text{Fe}(\text{CN})_6]^{4-}$  was blocked by both the cellular membrane and the substrate. At the cell edge, some strong negative feedback effect was seen. This is because the cell edge only partially blocked the diffusion of the  $[\text{Fe}(\text{CN})_6]^{4-}$ . SECM/SICM can detect the electrochemical current response produced by the surface heterogeneity.  $\text{FcCH}_2\text{OH}$  is a hydrophobic mediator that can cross the cell membrane.<sup>18</sup> When monitoring the oxidation current of  $\text{FcCH}_2\text{OH}$  (positive value), the current decreased as the probe approached the sample surface, due to the slight negative feedback effects. However, similar to oxygen, the  $\text{FcCH}_2\text{OH}$  oxidation current at the cellular membrane surface was large, compared to that at the substrate surface, because the cellular membrane is permeable for  $\text{FcCH}_2\text{OH}$  (Figure 9C right image). The larger oxidation current may also be caused by regeneration of  $\text{FcCH}_2\text{OH}$  inside the cellular processes.<sup>7</sup> The possibility of steady-state diffusion layer of



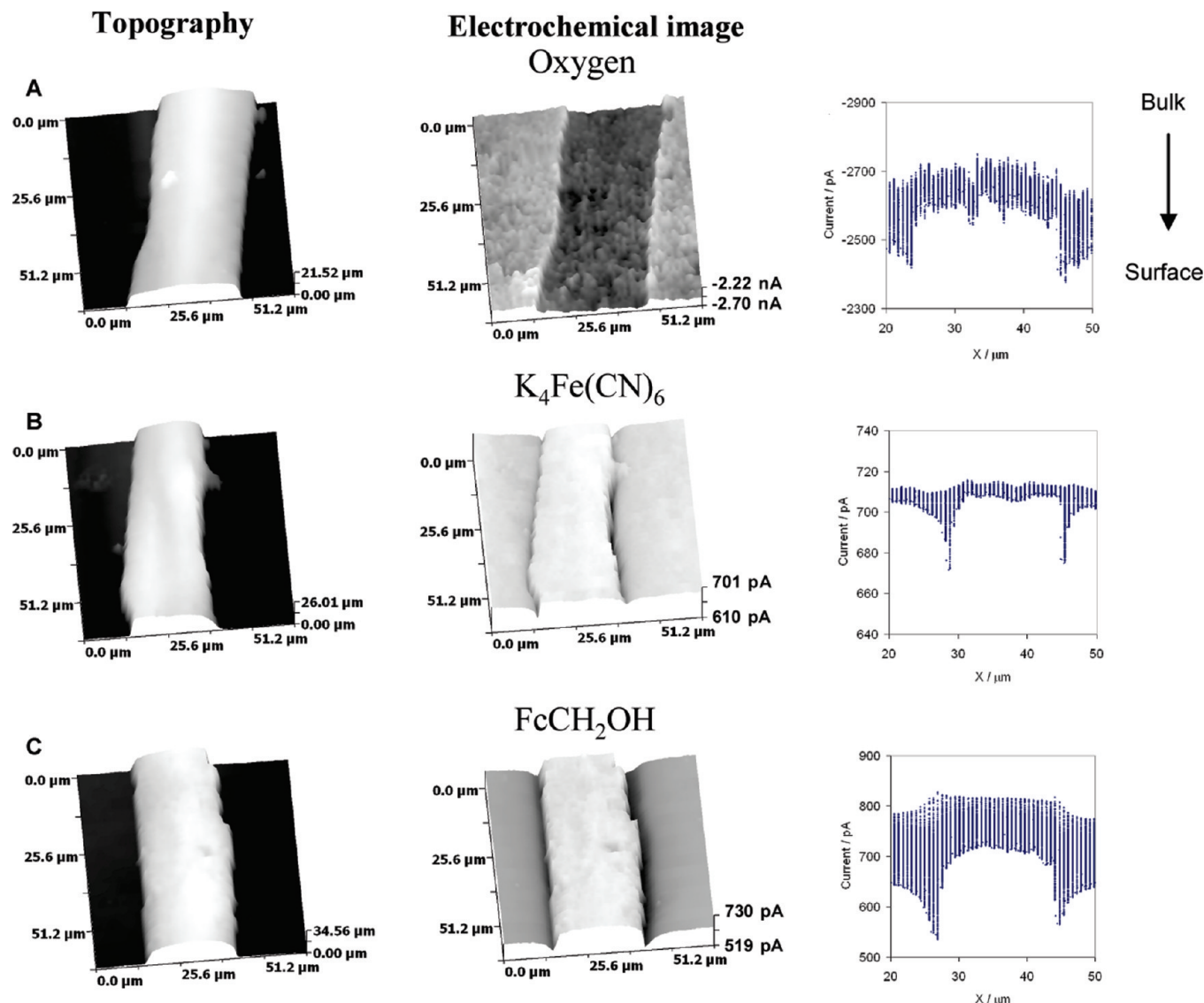


**Figure 9.** Topographic (left) and electrochemical (center) images of a rat cardiac myocyte and electrochemical signal profiles of repeated approach curves at each measurement point (right). Electrochemical images were based on (A) reduction current of oxygen at  $-500$  mV vs Ag/AgCl, (B) oxidation current of  $0.50$  mM  $\text{K}_4\text{Fe}(\text{CN})_6$  at  $500$  mV vs Ag/AgCl, and (C) oxidation current of  $0.50$  mM  $\text{FcCH}_2\text{OH}$  at  $500$  mV vs Ag/AgCl. The SICM nanopipette electrode was held at  $200$  mV vs Ag/AgCl. Scan ranges were  $64 \mu\text{m} \times 64 \mu\text{m}$ . The approach distances were set to  $10 \mu\text{m}$ . Arrows and dashed lines denote the direction of the approach and boundaries of the cell and substrate, respectively.

$\text{FcCH}_2\text{OH}$  associated with the cellular inner enzyme activity was detected. This is the first time that simultaneous characterization of the localized permeation property of a living cell membrane and cellular surface topography imaging was achieved. In our experiment, strict estimation of membrane permeability is difficult because the complicated shape of the electrode used. However, it is possible to compare the membrane permeation property, by using same electrode under the same experimental conditions.

## Conclusion

We developed a SECM/SICM system with a hybrid nanoprobe consisting of a nanoring electrode for electrochemical measurements and a nanopipette for ion current measurement as a feedback signal. This system enables simultaneous sub-micrometer scale electrochemical and noncontact topography measurements. Furthermore, we adopted the hopping scanning mode for ion current distance regulation to achieve convoluted living cellular surface topography measurements and detection

of the spatial distribution of electrochemical species. The present system will be applicable to detailed analysis of membrane surface phenomena that are induced by a nanopipette providing specific biomolecules locally.

**Acknowledgment.** This work was partly supported by a Grant-in-Aid for Scientific Research (18101006) from MEXT (Ministry of Education, Culture, Sports, Science and Technology), Japan. Y.T. acknowledges the support obtained from a research fellowship of the Japan Society for the Promotion of Science.

**Supporting Information Available:** The evaluation of the interference of the SECM nanoring electrode and SICM nanopipette electrode. SECM/SICM topography image comparison with AFM image. This material is available free of charge via the Internet at <http://pubs.acs.org>.

JA1029478